J Mater Sci (2019) 54:5412–5423

Chemical routes to materials

Facile in situ fabrication of Co nanoparticles embedded in 3D N-enriched mesoporous carbon foam electrocatalyst with enhanced activity and stability toward oxygen reduction reaction

Chunyang Xu[1], Zheng Lin[2], Dian Zhao[1], Yulin Sun[1], Yijun Zhong[1,*], Jiqiang Ning[3,*], Changcheng Zheng[4], Ziyang Zhang[3], and Yong Hu[1,*]

[1] *Key Laboratory of the Ministry of Education for Advanced Catalysis Materials, Department of Chemistry, Zhejiang Normal University, Jinhua 321004, China*

[2] *School of Materials Science and Engineering, Beihang University, Beijing 100191, China*

[3] *Vacuum Interconnected Nanotech Workstation, Suzhou Institute of Nano-Tech and Nano-Bionics, Chinese Academy of Sciences, Suzhou 215123, China*

[4] *Mathematics and Physics Centre, Department of Mathematical Sciences, Xi'an Jiaotong-Liverpool University, Suzhou 215123, China*

Received: 7 October 2018
Accepted: 12 December 2018
Published online: 2 January 2019

ABSTRACT

Oxygen reduction reaction (ORR) is a crucial reaction for various energy conversion and storage devices, but the sluggish kinetics and the usage of noble metals greatly restrict its practical device applications. In this work, a well-designed high-performance catalyst for ORR was synthesized via a facile one-step Co-MOF carbonization method, in which Co-MOF was prepared using the cobalt acetate tetrahydrate and 2,2′-bipyridyl-5,5′-dicarboxylic acid (H_2bpydc) as the only raw materials and H_2bpydc as the favorable carbon and nitrogen source for in situ nitrogen doping and metallic cobalt reduction. The resultant 3D mesoporous carbon foam catalyst with embedded Co nanoparticles (CoN–CF) is enriched with nitrogen, which exhibits high specific surface area and abundant N-doping active sites for catalytic ORR. In particular, the optimized CoN–CF-700 sample displays the best catalytic performances including onset potential of 0.94 V, half-wave potential of 0.85 V, long-term durability and superior resistance to methanol poisoning. The demonstrated synthetic strategy provides a new insight into easy-synthesis and high-economy routes for metal–N–C catalysts and a deeper understanding of the effects of microstructures on catalytic mechanisms.

Address correspondence to E-mail: yjzhong@zjnu.edu.cn; jqning2015@sinano.ac.cn; yonghu@zjnu.edu.cn; yonghuzjnu@163.com

https://doi.org/10.1007/s10853-018-03255-0

Introduction

The oxygen reduction reaction (ORR) plays an essential role in various environment-friendly and energy-saving technologies, such as rechargeable metal–air batteries, fuel cells and water splitting catalysts, which have been regarded as promising alternatives to traditional fossil fuels [1–3]. Nevertheless, the intrinsic sluggish kinetics dramatically restricts its practical applications. Although noble platinum (Pt) and its composites are acknowledged as the most effective ORR catalysts, the rarity, high cost and insufficient stability limit their large-scale applications [4, 5]. Therefore, it is highly desired to exploit earth-abundant and fast-kinetics alternatives to replace Pt-based catalysts [6, 7]. To date, magnificent progress has been made in developing new electrocatalysts, such as transition metal-based materials (metals and metal compounds MX, X=O, S, N, C, and P) [8–12] and heteroatom-doped carbon materials [13–17]. Particularly, it is noteworthy that transition metals (Co or Fe) embedded in N-doped carbon materials exhibit outstanding electroactivity for ORR [6, 18–26]. On the one hand, carbon frame with high conductivity works as a perfect supporting material with numerous active sites [27]. On the other hand, heteroatom doping, especially the N-doping, leads to more active centers for catalyzing ORR [28, 29]. However, the reported methods for N-doped carbon material synthesis encounter the common difficulty in controlling the structure of the carbon foam as well as doping uniformity. It therefore remains a great challenge to develop a facile strategy for controllable synthesis of this kind of hybrid catalysts.

As an optimal precursor to acquire porous carbon materials, metal–organic frameworks (MOFs), coordinating metal centers with organic ligands, have received intensive research interest [30–33]. The morphology, composition and pore size can be easily controlled by modifying the metal ions and organic ligands. In addition, the MOF-derived materials can also inherit the advantages of MOFs, such as porous structures with high specific surface area and uniform heteroatom doping [34–37], which are merits for high-performance catalysts toward ORR [16]. Such controllable synthetic method is hence expected to construct desirable metal–N–C hybrid materials with well-defined MOF precursors to achieve superior ORR activity.

However, most reported MOFs are neither uniform in size nor stable at high temperatures, which greatly impedes its application for high-performance MOF-derived electrocatalysts. For example, the Co–N–C catalysts derived from cobalt zeolitic imidazolate framework (Co-ZIF) showed good ORR activity due to the synergy of N and Co and the porous structures [28, 37, 38], but the ORR activity is difficult to be further promoted for the instability of 2-methylimidazole ligand and the loss of N in the process of high-temperature pyrolysis. Besides, the synthesis of MOFs always involves long-reaction time of several days as well as low economical benefits [16, 33]. Therefore, a facile approach for the synthesis of MOF-derived porous Co–N–C materials with favorable N contents is highly desired.

In this work, we have developed a novel high-activity electrocatalyst for ORR, which consists of Co nanoparticles (NPs) embedded in 3D N-enriched mesoporous carbon foam (depicted as CoN–CF). The designed Co-MOF precursor was assembled by using 2,2′-bipyridyl-5,5′-dicarboxylic acid (H_2bpydc) ligands with Co cations through a facile reflux method, in which the H_2bpydc ligand acts as the favorable N and C sources for the N-doped carbon foam, and the multi-N doping can be controlled by simply adjusting the pyrolyzing temperature. The CoN–CF-700 catalyst obtained at middle pyrolyzing temperature with dominant content of pyridinic-N and graphitic-N displays the best catalytic activity for ORR. Specifically, the CoN–CF-700 sample exhibits excellent catalytic performance, including high onset potential of 0.94 V, half-wave potential of 0.85 V and limiting current density of -5.24 mA cm^{-2}. Moreover, this catalyst also exhibits better resistance to methanol poisoning and distinct long-term stability compared with commercial Pt/C catalysts. We believe that this demonstrated strategy provides an easy route for the synthesis of metal–N–C catalysts with controllable active sites for high-efficiency ORR applications.

Experimental section

Synthesis of Co-MOF

The Co-MOF precursor was prepared by refluxing at 85 °C for 9 h with 200 mg cobalt acetate tetrahydrate and 50 mg 2,2′-bipyridyl-5,5′-dicarboxylic acid dissolved in a mixed solution of 12 mL HNO_3 (2.8 M in DMF), 20 mL DMF, 20 mL H_2O, 20 mL CH_3CN [39]. The Co-MOF was collected by centrifugation and washed with deionized water before being dried at 80 °C.

Synthesis of CoN–CF catalysts

The Co-MOF precursor was directly carbonized in N_2 in a tube furnace which was heated with a rate of 2 °C min^{-1} to certain temperature and then maintained for 2 h. With the heating temperature of 600, 700 and 800 °C, the CoN–CF-600, CoN–CF-700 and CoN–CF-800 samples were obtained, respectively. The as-obtained products were treated with 0.5 M H_2SO_4 for 10 h to remove the unstable and inactive substances, and then washed several times with deionized water and finally dried at 80 °C. For the aim of comparison, NC-700 sample was prepared without using cobalt acetate tetrahydrate.

Material characterization

The crystalline phase and purity of the as-prepared samples were analyzed by the technique of powder X-ray diffraction (XRD) with a Philips PW3040/60 X-ray diffractometer using Cu–Ka radiation. The morphologies of the samples were examined by scanning electron microscopy (SEM) on a Hitachi S-4800 scanning electron micro-analyzer with an accelerating voltage of 5 kV. The microstructure of the samples was characterized by transmission electron microscopy (TEM) and high-resolution TEM (HRTEM) with a JEM-2100 Field emission TEM. The surface compositions and chemical states the samples were analyzed with X-ray photoelectron spectroscopy (XPS) on an ESCALab MKII X-ray photoelectron spectrometer using Mg Ka X-ray as the excitation source. N_2 adsorption isotherms were performed at 77 K on a Micrometrics ASAP 2020 surface area and porosity analyzer after the sample was degassed in vacuum at 300 °C for 4 h.

Electrochemical measurements

The ORR performance of the as-prepared samples was measured with a three-electrode cell using WaveDriver 20 bipotentiostat (Pine Instrument Company, USA). A saturated calomel electrode (SCE, saturated KCl) and a Pt foil were used as the reference electrode and counter electrode, respectively. All measured potentials in this work were converted to the reversible hydrogen electrode (RHE) according to the equation: E (RHE) = E (SCE) + 0.059 × pH + 0.241. A rotating disk electrode (RDE) with a glass carbon disk (5 mm in diameter) and a rotating ring-disk electrode (RRDE) with a Pt ring (6.5 mm in inner diameter and 8.5 mm in outer diameter) and a glass carbon disk (5.5 mm in diameter) coated with the catalyst film were used as the working electrodes. Five milligrams of the catalyst was dispersed in 460 μL of ethanol and 40 μL of 5% Nafion solution to get the catalyst ink. The mixture was sonicated for at least 1 h to obtain a uniform suspension. A certain volume of catalyst ink was cast onto the glass carbon substrate with the catalyst loading of 0.2 mg cm^{-2} for all samples including the commercial Pt/C (20 wt% on carbon black, Alfa Aesar), which was finally dried under ambient conditions. The electrolyte was 0.1 M KOH solution, which was purged with O_2 or N_2 flow for at least 30 min. The CV tests were conducted in the O_2- or N_2-saturated electrolyte from 0 to 1.2 V versus RHE with a scan rate of 20 mV s^{-1}. And the RDE tests were carried out in O_2-saturated electrolyte with a scan rate of 10 mV s^{-1} from 1.2 to 0.2 V versus RHE. The methanol poisoning tests were performed by chronoamperometry at the potential of 0.6 V versus RHE by RDE tests, with 50 mL of methanol introduced into 150 mL of 0.1 M KOH solution. The electron transfer number can be calculated according to the *K–L* equation at various potentials as follows:

$$\frac{1}{j} = \frac{1}{j_L} + \frac{1}{j_K} = \frac{1}{B\omega^{1/2}} + \frac{1}{j_K} \quad (1)$$

$$B = 0.2nFAC_0D_0^{2/3}v^{-1/6} \quad (2)$$

where j is the measured current density, j_K and j_L are the kinetic and limiting current densities, respectively, ω is the rotating speed (rpm), n is the electron transfer number, F is the Faraday constant (96485 C mol^{-1}), C_0 is the bulk concentration of O_2 (1.2×10^{-3} mol L^{-1}), D_0 is the diffusion coefficient of

O_2 (1.9×10^{-5} cm^2 s^{-1}), and ν is the kinematic viscosity of the electrolyte (0.01 cm^2 s^{-1}).

The RRDE measurements were performed at voltage ranging from 0.2 to 1.2 V versus RHE in O_2-saturated electrolyte, with a scan rate of 10 mV s^{-1} at a rotation speed of 1600 rpm. The yield of H_2O_2 and the electron transfer number could be determined according to the following equations:

$$H_2O_2\% = 200\frac{I_r/N}{I_d + I_r/N} \quad (3)$$

$$n = 4\frac{I_d}{I_d + I_r/N} \quad (4)$$

where I_d is the disk current, I_r is the ring current, and N is the collection efficiency of the ring electrode which was 0.37 as provided by the manufacturer.

Results and discussion

The synthesis of the CoN–CF catalysts by a novel reflux method, followed by a carbonization process at certain temperature, is illustrated in Scheme 1. H_2-bpydc, N-heterocyclic carboxylate ligand, was selected as the source for both carbon and nitrogen, which can be decomposed into CO_2 and H_2O during the carbonization process resulting in the mesoporous N-doped graphite carbon layers. Meanwhile, cobalt acetate tetrahydrate was reduced to metallic Co NPs which coordinate with the graphite carbon, leading to the embedding of Co NPs in the 3D N-enriched mesoporous carbon foam.

The morphology and structure of the obtained catalysts were investigated by SEM and TEM. As shown in Fig. S1 (see Supplementary Materials), the as-prepared CoN–CF gets much rougher than the Co-MOF precursor, due to the growth of small particles on the smooth surface. Obviously, more holes and voids emerge in CoN–CF-800 than CoN–CF-600, indicating the effect of pyrolysis temperature on the formation of the porous 3D carbon frame. Such porous structure is also confirmed by the TEM images. As displayed in Fig. 1a, b, numerous voids can be observed clearly. In Fig. 1a–d and Fig. S3a–d, the CoN–CF-700 sample exhibits the existence of graphitic carbon bubbles and metallic Co NPs embedded in the carbon layers, which were further confirmed by the HRTEM images. In Fig. 1e, the inner particle exhibits an inter-planar spacing of 0.2 nm which corresponds to the distance of the (111) plane of metal Co, and the outer shell shows a spacing of 0.34 nm corresponding to the (002) plane of graphitic carbon. It was noteworthy that Co NPs still remain even after high-temperature calcination and acid-washing. Such metallic Co NPs were encapsulated by the graphitic carbon layers ranging from 6 to 8 layers or from 10 to 14 layers (Fig. S3c–d). As observed in the TEM images (Fig. S3), the graphitic carbon layers are ultra-thin and imperfect, resulting in the Co NPs are only partially encapsulated in carbon layers. Therefore, the

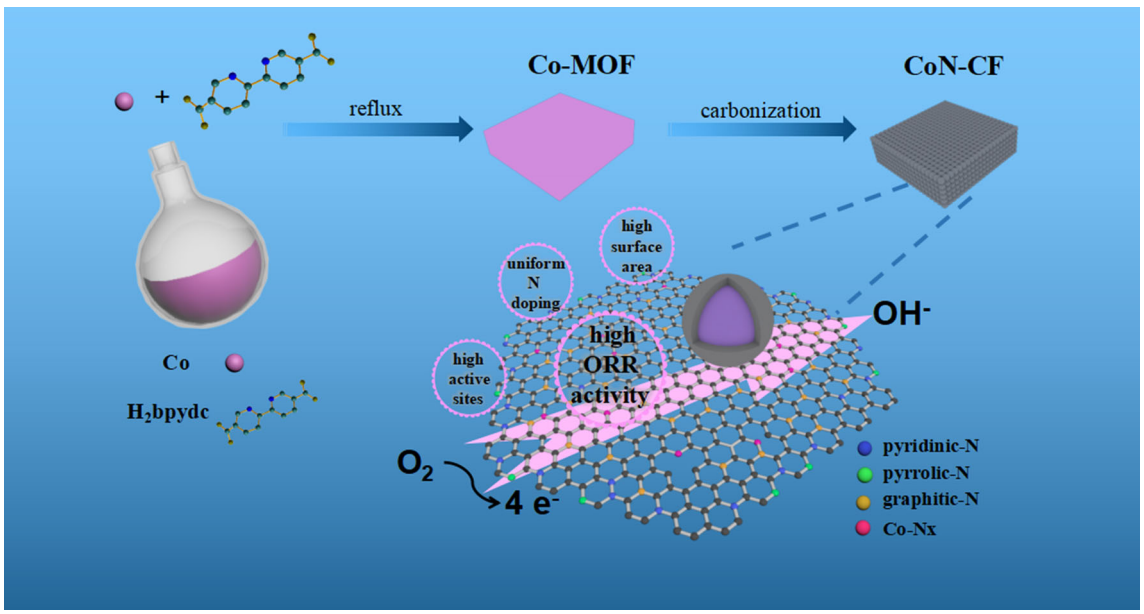

Scheme 1 The schematic procedure for the synthesis of CoN–CF.

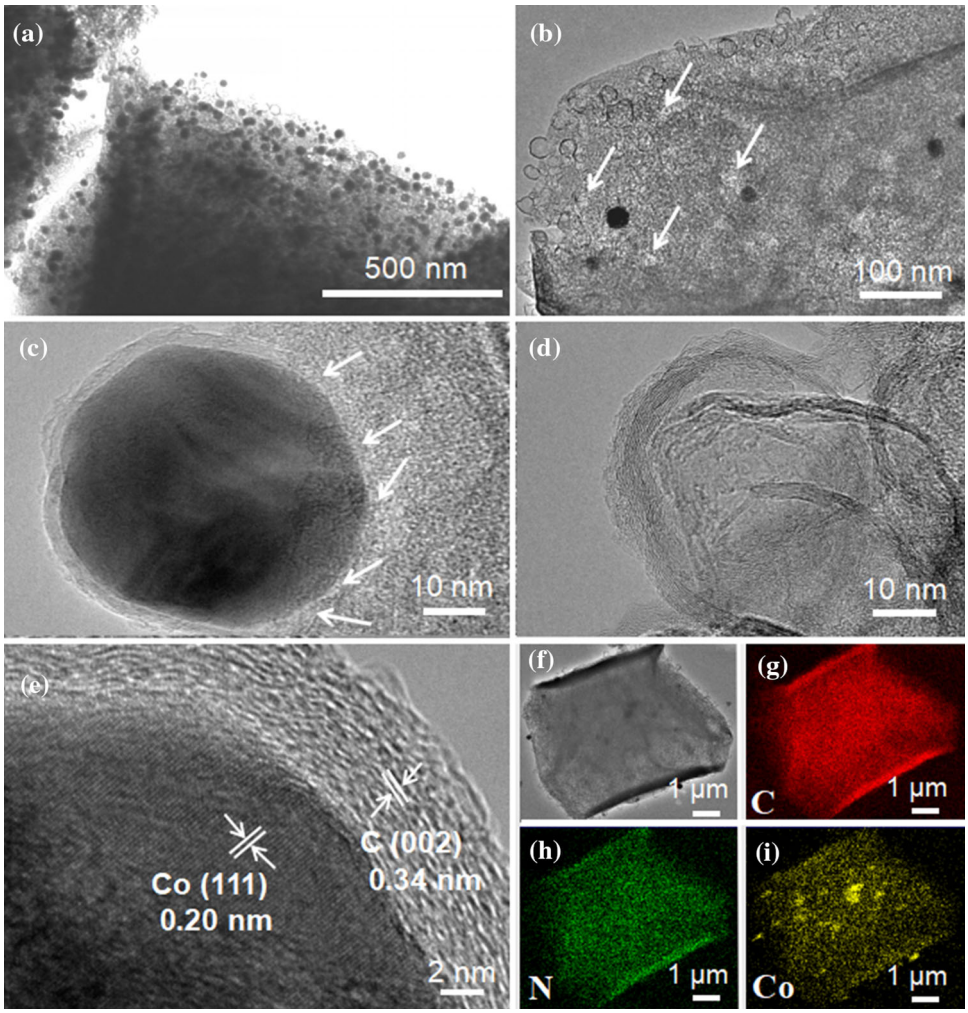

Figure 1 **a–d** TEM, **e** HRTEM image, and **f** STEM image of the as-prepared samples CoN–CF-700; **g–i** elemental mapping images of C, N and Co elements, respectively. The arrows noted in the **b** and **c** represent the pores.

electrolyte can penetrate through the outside carbon layers to the inside metal NPs. Additionally, there are many pores distributed in the N-doped carbon layers (noted as the arrows in the Fig. S3c–f); thus, the electrolyte can also interact with the Co NPs through the pores in the carbon layers. Such core–shell structure of Co NPs encapsulated by graphitic carbon layers with unique structural advantages not only can improve the ORR performance by dual physical and chemical protection but also works as conduction paths and reactive sites in the electrocatalytic process. Moreover, all the C, N and Co elements were uniformly distributed over the whole carbon foam as shown in Fig. 1g–i. The above SEM and TEM inspections have revealed that the porous 3D N-enriched carbon foam with embedded Co NPs was successfully obtained. Such unique structure is expected to not only possess high active sites but also have long-term catalytic stability for the well-protected Co NPs by graphitized carbon layers.

Further structure and composition characterizations were performed with XRD, Raman scattering spectroscopy and N_2 adsorption–desorption isotherms measurements. The XRD pattern of as-prepared Co-MOF (Fig. S2) is consistent well with the simulated pattern in the previous work [39], indicating the successful preparation of Co-MOF with this facile reflux method. In Fig. 2a, one broad peak at $2\theta \sim 25.5°$ and other three well-defined peaks at $2\theta \sim 44.1°$, 51.4° and 75.6° can be seen clearly related to the (002) face of graphite carbon and metallic Co (JCPDS card NO. 15-0806), respectively, which is in accord with the TEM results. And the peaks of CoO emerged in CoN–CF-800 are ascribed to the partially oxidized cobalt at 800 °C, which could be confirmed by the XPS analyses with the CoO bond in high-resolution Co 2*p* spectra of CoN–CF-800. The Raman

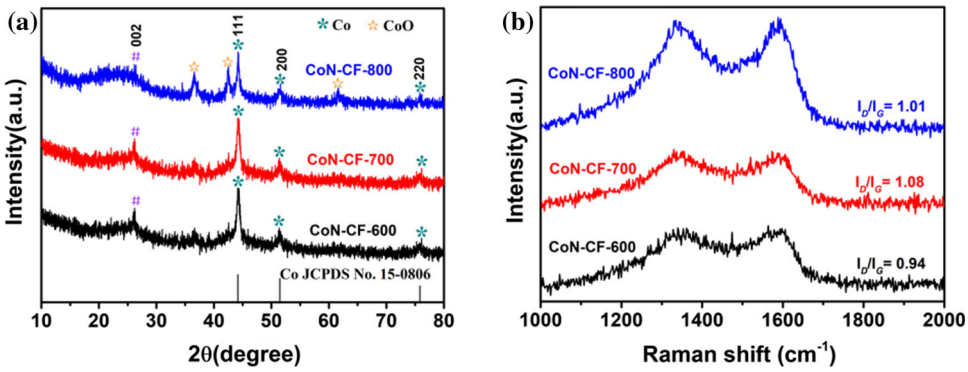

Figure 2 **a** XRD patterns. **b** Raman spectra of the as-prepared samples at different carbonization temperature.

spectra show the characteristic of the graphitic carbon and the ratio of I_D/I_G can be used to reveal the disordered and graphitic degree [40, 41]. As shown in Fig. 2b, two obvious peaks at 1340 cm^{-1} (*D* band) and 1595 cm^{-1} (*G* band) can be observed [42]. It is noticed that the I_D/I_G value of CoN–CF-700 (1.08) is higher than that of CoN–CF-600 (0.94) and CoN–CF-800 (1.01), implying that the sample calcined at 700 °C produced more structural defects [43]. Moreover, the surface area and porous structure were examined with N_2 adsorption–desorption tests. Figure 3a–c reveals a type-IV isotherm for the as-prepared samples calcined at different temperatures, indicating the existence of a mesoporous structure. The average pore size of CoN–CF-600 and CoN–CF-700 was centered at mesopores, while pore of CoN–CF-800 was centered at both mesopores and macropores which is also in accordance with their surface area [44]. The surface area of CoN–CF samples is more likely influenced by the calcination temperatures. The Brunauer–Emmett–Teller (BET) surface areas of CoN–CF-600, CoN–CF-700 and CoN–CF-800 are 544.6, 593.1 and 835.7 $m^2\ g^{-1}$ (Fig. 2d), respectively, which are much higher than the values of reported catalysts [45–51]. The increased surface area may mainly result from the increased mesopores and macropores at higher temperatures. The specific surface area has been regarded as one of the crucial

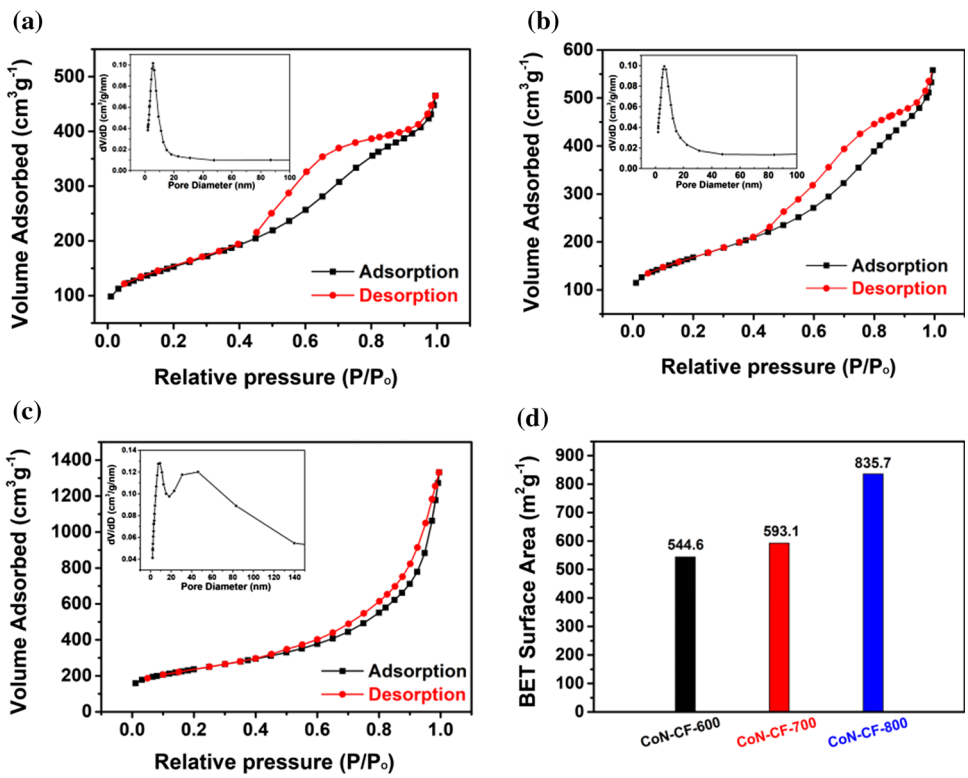

Figure 3 **a**, **b** and **c** N_2 adsorption–desorption isotherms of the as-prepared CoN–CF-600, CoN–CF-700 and CoN–CF-800 samples. **d** BET surface area of the as-prepared samples at different carbonization temperature. The insets in **a**, **b** and **c** show the corresponding pore size distribution curve.

factors to influent the ORR performance, and a larger surface area is expected to provide more active sites, resulting in a higher electrocatalytic activity. Such unique 3D porous carbon foam with ultrahigh specific surface area is a result of the high coordination between H_2bpydc with Co as well as the gas releasing from decomposition at high temperatures, which is expected to facilitate relevant species transport and expose more active sites in the electrochemical reactions.

XPS measurements were also conducted to examine the elemental compositions and chemical states of the CoN–CF catalysts. The survey XPS spectrum (Fig. 4a) confirms the presence of C, N, O, Co in all the catalysts, which is in agreement with the TEM elemental mapping, and the corresponding atomic percentages are shown in Table S1 (see Supplementary Materials). Obviously, the total content of N decreases rapidly from 6.33% in CoN–CF-600 to 4.13% in CoN–CF-700 and 1.29% in CoN–CF-800. However, the highest content of Co is obtained in CoN–CF-700 (3.73%), much higher than in CoN–CF-600 (2.07%) and CoN–CF-800 (0.51%), implying uniformly distributed Co. Recent research has confirmed that both N and Co play a vital role in the ORR performance [17, 28, 52], and a small amount of metallic Co can improve the electrocatalytic activity toward ORR [25]. The presence of Co can lead to formation of Co–N species which is proposed as the catalytic site. Meanwhile, metal Co can catalyze graphitization of amorphous carbon to generate graphitic carbon [25]. In Fig. 4b, the high-resolution C 1*s* spectrum of CoN–CF-700 can be deconvoluted into three fitting peaks, corresponding to C=C (284.4 eV), C=N & C–O (285.1 eV) and C–N & C=O (287.9 eV), [48], respectively, revealing the successfully doped of N in the carbon foam. The corresponding C 1*s* spectra of CoN–CF-600 and CoN–CF-800 are shown in Fig. S4a and S4c. In the high-resolution Co 2*p* spectra of CoN–CF-700 (Fig. 4c) and CoN–CF-600 (Fig. S4b), two distinct peaks at the binding energies of ~ 793.8 and 778.4 eV can be attributed to metallic Co $2p_{1/2}$ and $2p_{3/2}$, and the peak at ~ 779.9 eV can be ascribed to the Co–N bond [53, 54]. The binding energy for Co–O bond at ~ 787.2 eV could be detected in the Co 2*p* spectrum of CoN–CF-800, which is in agreement with the XRD results. In Fig. 4e, the high-resolution N 1*s* spectrum exhibits four sub-peaks, including pyridinic-N (398.3 eV), pyrrolic-N (400.3 eV), graphitic-N (401.5 eV) and Co–N (399.2 eV) for all CoN–CF samples [45, 53, 55, 56]. Specifically, the contents of different N are shown in Fig. 4d and Table S2. It has been generally acknowledged that pyridinic-N and graphitic-N contribute a lot to electrocatalytic activities [15, 28, 57–61], and pyrolyzing temperature can influence the different N

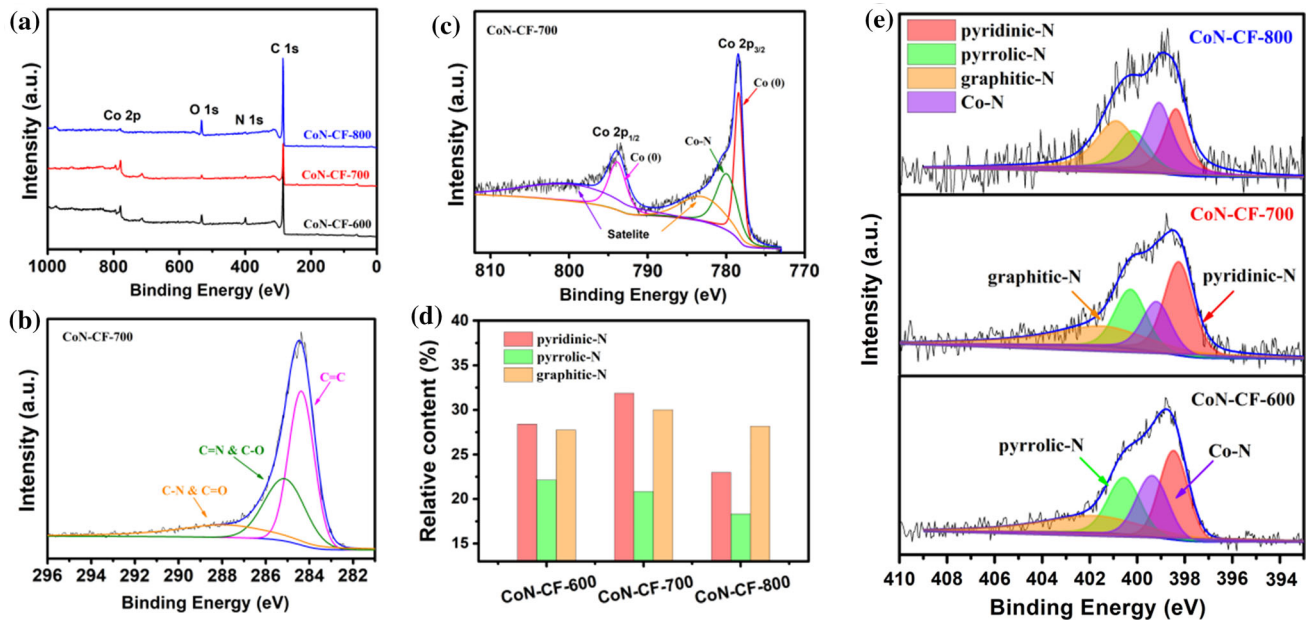

Figure 4 **a** The wide XPS survey spectra of as-prepared samples, **b** high-resolution C 1*s* spectra and **c** high-resolution Co 2*p* spectra of CoN–CF-700, **d** relative content of different N components and **e** High-resolution N 1*s* spectra of as-prepared samples.

content in this case. At 600 °C, the CoN–CF-600 sample contains 28.41% pyridinic-N and 27.75% graphitic-N. When the temperature rises to 700 °C, the contents of pyridinic-N and graphitic-N are increased to 31.86% and 30.12%, respectively. However, the CoN–CF-800 sample has only about 22.98% pyridinic-N and 28.17% graphitic-N. It is noted that the both pyridinic-N and graphitic-N contents appear to decrease as temperature is increased to 800 °C, which may be attributed to the thermal instability of the pyridinic and graphitic groups at higher annealing temperatures [61]. In general, the graphitic-N content is related to conductivity of N-doped carbons which determines the limiting current density, while the pyridinic-N content will enhance the onset potential for ORR [25, 61]. Thus, the CoN–CF-700 catalyst obtained at middle pyrolyzing temperature with dominant content of pyridinic-N and graphitic-N exhibits the best electrocatalytic activity in the following catalytic examination.

These features of high specific surface area, rich nitrogen doping and uniform Co distribution make CoN–CF a promising ORR catalyst. The electrocatalytic activity of CoN–CF samples was investigated by linear sweep voltammetry (LSV) and cyclic voltammetry (CV) measurements on a rotating disk electrode (RDE) in 0.1 M KOH electrolyte. Linear sweep voltammetry (LSV) measurements with a rotating speed of 1600 rpm were implemented to evaluate the ORR activities of the CoN–CF and Pt/C catalysts. The obtained LSV curves and the corresponding ORR activity parameters are presented in Fig. 5a–b and Table S3. As expected, the CoN–CF-700 sample exhibits the best ORR activity with a higher onset potential (E_{onset}, 0.94 V) and a more positive half-wave potential ($E_{1/2}$, 0.85 V) than CoN–CF-600 (0.89 V, 0.82 V) and CoN–CF-800 (0.92 V, 0.83 V) samples, which is even better than the Pt/C (0.93 V, 0.84 V) catalyst. Besides, CoN–CF-700 also displays a higher limiting current density of − 5.24 mA cm^{-2} than Pt/C (− 4.98 mA cm^{-2}). As for NC-700 catalyst without Co NPs, poor ORR performance with rather low current density was observed. This result confirms that the introduction of metal Co significantly enhanced the ORR activity, which in turn verifies that the Co nanoparticles encapsulated in graphitic carbon can become the active sites to boost ORR. Thus, the carbonization temperature of 700 °C is the optimal temperature for the best catalytic performance of the CoN–CF catalysts. Figure 5c exhibits the CV results of CoN–CF-700 in O_2 and N_2-saturated electrolytes, where a distinct reduction peak is seen in the O_2-saturated electrolyte, while no noticeable peak can be observed in the N_2-saturated electrolyte, demonstrating the encouraging response toward ORR of the CoN–CF-700 catalyst [42]. Moreover, LSV tests at different rotation rates (Fig. 5d) were also performed and the limiting current density demonstrates a regular increase with the increased rotation rates owing to the shorter ion diffusion path at high rates [62]. The corresponding Koutecky–Levich (*K–L*) curves (the inset plot in Fig. 5d, according to Eqs. 1, 2) indicate a good linearity with the growing potentials and the transferred electron number is calculated to be ~ 3.9. To further investigate the reaction process of ORR, the RRDE test was performed with a rotation rate of 1600 rpm. The LSV curves of the CoN–CF-700 and Pt/C catalysts were presented in Fig. S6, and the electron transfer number of CoN–CF-700 is calculated to be ~ 3.95 which further confirms a four electron ($4e^-$) ORR process. The yield of H_2O_2 was also calculated according to the Eq. 3 and the production is below 4.0%, indicating excellent catalytic selectivity to reduce O_2 to H_2O instead of H_2O_2 [57] All these results demonstrate the highest catalytic performance of the CoN–CF-700 sample.

The as-prepared CoN–CF-700 sample was further tested to investigate its tolerance to methanol poisoning and long-term stability. The CoN–CF-700 sample as well as the Pt/C catalyst was measured in O_2 saturated 0.1 M KOH solution with rapid injection of 50 mL methanol in 300 s. As depicted in Fig. 4e, a great decline of the current density of Pt/C occurs with the introduction of 50 mL methanol into 0.1 M KOH solution, but for CoN–CF-700 sample, the relative current changes a little at the adding of methanol and recovers very quickly, which indicates stronger resistance of the CoN–CF-700 sample to methanol poisoning than the Pt/C. Furthermore, the catalytic durability of CoN–CF-700 and Pt/C was evaluated by chronoamperometric test performed at 0.6 V for a time period of 36000 s (Fig. 4f). Obviously, the current density of Pt/C drops dramatically and remains only 40.5% at the end of the test, while the CoN–CF-700 catalysts displays only a slight decline of the current density and a final retention of 96.7% after 36000 s. In addition, the LSV test of CoN–CF-700 after 3000 CV cycles was also performed, and only a small shift of 10 mV can be observed (Fig. S7). Compared with the Pt/C catalyst and other non-

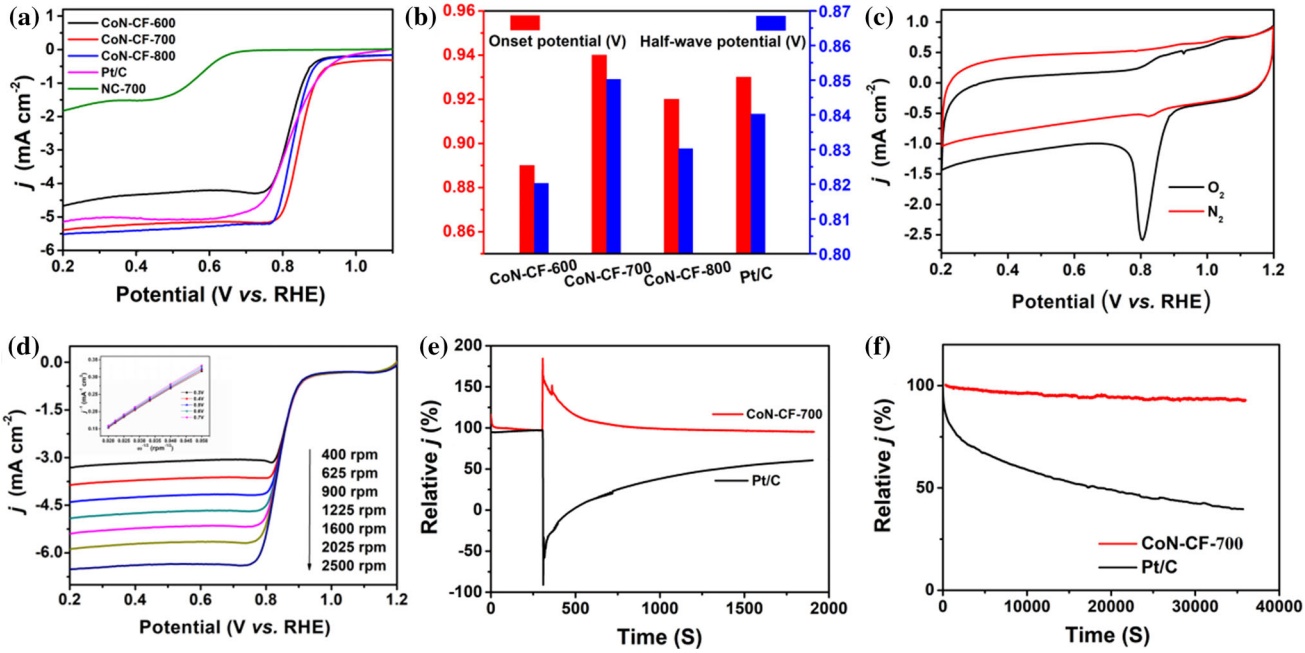

Figure 5 **a** LSV curves of CoN–CF-600, CoN–CF-700, CoN–CF-800, Pt/C and NC-700. **b** The onset potential and half-wave potential of CoN–CF-600, CoN–CF-700, CoN–CF-800, Pt/C. **c** CV curves of CoN–CF-700 (the red curve was obtained in N_2-saturated 0.1 M KOH solution, the black curve was obtained in O_2-saturated 0.1 M KOH solution). **d** LSV curves of CoN–CF-700 at different rotation rates. The inset in **d** shows the corresponding *K–L* plots at different potentials. **e** Chronoamperometric response at 0.6 V in O_2 saturated 0.1 M KOH solution with the adding of 50 mL methanol. **f** Chronoamperometric response of Pt/C and CoN–CF-700 at 0.6 V.

noble metal catalysts (Table S4), the as-prepared CoN–CF-700 sample exhibits superior ORR performance, including the higher onset potential, half-wave potential and limiting current density as well as strong resistance to methanol poisoning and distinct long-term stability. Such remarkably improved electrocatalytic activity of the CoN–CF-700 sample could be ascribed to the following factors: (1) Observed from SEM and BET results, the unique 3D porous structure not only offers high specific surface area with uniform N-doping but also facilitates the ion diffusion and charge carrier transfer at the interface of the electrolyte and electrode; (2) TEM images show that the embedded Co NPs are well dispersed in the graphitized carbon layers, which effectively prevents the agglomeration of the nanoparticles and guarantees the long-term stability of the catalyst in the electrochemical reaction; (3) As confirmed by XPS measurements, the in situ doping of multi-N components in the carbon foam results in abundant highly active sites and dominant content of pyridinic-N and graphitic-N and therefore the superb ORR performance.

Conclusions

In summary, we have demonstrated the synthesis of a well-designed high-performance ORR catalyst through a method of one-step carbonization of Co-MOF. The Co-MOF was synthetized by a facile reflux method in which only cobalt acetate tetrahydrate and H_2bpydc were used as the raw materials. The carbonization of the H_2bpydc ligands leads to in situ N-doping into the carbon foam as well as the reduction of Co cations to produce metallic Co NPs. The 3D N-enriched porous carbon foam with embedded Co NPs possesses high specific surface area and abundant N-doping active sites and exhibits high catalyst activity for ORR. In particular, the optimized CoN–CF-700 catalyst displays the best catalytic performance with an onset potential of 0.94 V, half-wave potential of 0.85 V and high limiting current density of − 5.24 mA cm^{-2}. Moreover, the CoN–CF-700 sample also shows superior resistance to methanol poisoning and remarkable long-term durability. We believe the demonstrated strategy not only realizes the unique 3D structural features with superior electrocatalytic activity but also

provides a new insight into easy-synthesis and high-economy routes for developing metal–N–C catalysts for energy storage and conversion applications.

Acknowledgements

Y. Hu acknowledges the financial support from Natural Science Foundation of China (21671173). J. Q. Ning acknowledges the financial support from Natural Science Foundation of China (11874390), Cutting-edge Key Research Program of Chinese Academy of Sciences (QYZDB-SSW-JSC014) and Hundred Talents Program of Chinese Academy of Sciences.

Electronic supplementary material: The online version of this article (https://doi.org/10.1007/s10853-018-03255-0) contains supplementary material, which is available to authorized users.

References

[1] Cao X, Tan C, Sindoro M, Zhang H (2017) Hybrid micro-/nanostructures derived from metal–organic frameworks: preparation and applications in energy storage and conversion. Chem Soc Rev 46:2660–2677

[2] Chu S, Majumdar A (2012) Opportunities and challenges for a sustainable energy future. Nature 488:294

[3] Debe MK (2012) Electrocatalyst approaches and challenges for automotive fuel cells. Nature 486:43

[4] Fan Z, Zhang H (2016) Crystal phase-controlled synthesis, properties and applications of noble metal nanomaterials. Chem Soc Rev 45:63–82

[5] Nie Y, Li L, Wei Z (2015) Recent advancements in Pt and Pt-free catalysts for oxygen reduction reaction. Chem Soc Rev 44:2168–2201

[6] Wu G, More KL, Johnston CM, Zelenay P (2011) High-performance electrocatalysts for oxygen reduction derived from polyaniline, iron, and cobalt. Science 332:443

[7] Song P, Luo M, Liu XZ, Xing W, Xu WL, Jiang Z, Gu L (2017) Zn single atom catalyst for highly efficient oxygen reduction reaction. Adv Funct Mater 27:1700802

[8] Feng Y, Xu C, Hu E, Xia B, Ning J, Zheng C, Zhong Y, Zhang Z, Hu Y (2018) Construction of hierarchical FeP/Ni_2P hollow nanospindles for efficient oxygen evolution. J Mater Chem A 6:14103–14111

[9] Sun D, Ye L, Sun F, García H, Li Z (2018) From mixed-metal MOFs to carbon-coated core–shell metal alloy@metal oxide solid solutions: transformation of Co/Ni-MOF-74 to Co_xNi_{1-x}@Co_yNi_{1-y}O@C for the oxygen evolution reaction. Inorg Chem 56:5203–5209

[10] Wang X, Yu L, Bu Y, Song S, Lou XW (2018) Metal–organic framework hybrid-assisted formation of Co_3O_4/Co–Fe oxide double-shelled nanoboxes for enhanced oxygen evolution. Adv Mater 30:1801211

[11] Hu E, Feng Y, Nai J, Zhao D, Hu Y, Lou XW (2018) Construction of hierarchical Ni–Co–P hollow nanobricks with oriented nanosheets for efficient overall water splitting. Energy Environ Sci 11:872–880

[12] Hu E, Ning J, Zhao D, Xu C, Lin Y, Zhong Y, Zhang Z, Wang Y, Hu Y (2018) A room-temperature postsynthetic ligand exchange strategy to construct mesoporous Fe-doped CoP hollow triangle plate arrays for efficient electrocatalytic water splitting. Small 14:1704233

[13] Jiao Y, Zheng Y, Jaroniec M, Qiao SZ (2015) Design of electrocatalysts for oxygen- and hydrogen-involving energy conversion reactions. Chem Soc Rev 44:2060–2086

[14] Zhang W, Wu ZY, Jiang HL, Yu SH (2014) Nanowire-directed templating synthesis of metal–organic framework nanofibers and their derived porous doped carbon nanofibers for enhanced electrocatalysis. J Am Chem Soc 136:14385–14388

[15] Yang HB, Miao J, Hung SF, Chen J, Tao HB, Wang X, Zhang L, Chen R, Gao J, Chen HM, Dai L, Liu B (2016) Identification of catalytic sites for oxygen reduction and oxygen evolution in N-doped graphene materials: development of highly efficient metal-free bifunctional electrocatalyst. Sci Adv 2:e1501122

[16] Ren Q, Wang H, Lu X, Tong Y, Li G (2018) Recent progress on MOF-derived heteroatom-doped carbon-based electrocatalysts for oxygen reduction reaction. Adv Sci 5:1700515

[17] Wang Y, Chen W, Chen Y, Wei B, Chen L, Peng L, Xiang R, Li J, Wang Z, Wei Z (2018) Carbon-based catalysts by structural manipulation with iron for oxygen reduction reaction. J Mater Chem A 6:8405–8412

[18] Bu Y, Lu Y, Wang Y, Wu M, Lou XW (2018) Porous iron–cobalt alloy/nitrogen-doped carbon cages synthesized via pyrolysis of complex metal–organic framework hybrids for oxygen reduction. Adv Funct Mater 28:1706738

[19] Hu E, Yu X, Chen F, Wu Y, Hu Y, Lou XW (2018) Graphene layers-wrapped Fe/Fe_5C_2 nanoparticles supported on N-doped graphene nanosheets for highly efficient oxygen reduction. Adv Energy Mater 8:1702476

[20] Li M, Bai L, Wu S, Wen X, Guan J (2018) Co/CoOx nanoparticles embedded on carbon for efficient catalysis of oxygen evolution and oxygen reduction reactions. Chem Sus Chem 11:1722–1727

[21] Li S, Cheng C, Liang H, Feng X, Thomas A (2017) 2D porous carbons prepared from layered organic–inorganic hybrids and their use as oxygen-reduction electrocatalysts. Adv Mater 29:1700707

[22] Fu X, Zamani P, Chio J, Hassan F, Jiang F, Higgins D, Zhang Y, Hoque M, Chen Z (2017) In situ polymer graphenization ingrained with nanoporosity in a nitrogenous electrocatalyst boosting the performance of polymer-electrolyte-membrane fuel cells. Adv Mater 29:1604456

[23] Zhan T, Lu S, Rong H, Hou W, Teng H, Wen Y (2018) Metal–organic-framework-derived Co/nitrogen-doped porous carbon composite as an effective oxygen reduction electrocatalyst. J Mater Sci 53:6774–6784. https://doi.org/10.1007/s10853-018-1989-x

[24] Kim H, Kim Y, Noh Y, Lee S, Sung J, Kim WB (2017) Thermally-converted CoO nanoparticles embedded into N-doped carbons as highly efficient bi-functional electrocatalysts for oxygen reduction and evolution reactions. Chem Cat Chem 9:1503–1510

[25] Hou Y, Wen Z, Cui S, Ci S, Shun Mao, Chen J (2015) An advanced nitrogen-doped graphene/cobalt-embedded porous carbon polyhedron hybrid for efficient catalysis of oxygen reduction and water splitting. Adv Funct Mater 25:872–882

[26] Tang H, Zeng Y, Zeng Y, Wang R, Cai S, Liao C, Cai H, Lu X, Tsiakaras P (2017) Iron-embedded nitrogen doped carbon frameworks as robust catalyst for oxygen reduction reaction in microbial fuel cells. Appl Catal B Environ 202:550–556

[27] Zhang Y, Ge J, Wang L, Wang D, Ding F, Tao X, Chen W (2013) Manageable N-doped graphene for high performance oxygen reduction reaction. Sci Rep 3:2771

[28] Chen Y, Wang C, Wu Z, Xiong Q, Xu Q, Yu SH, Jiang HL (2015) From bimetallic metal–organic framework to porous carbon: high surface area and multicomponent active dopants for excellent electrocatalysis. Adv Mater 27:5010–5016

[29] Xia B, Yan Y, Li N, Wu HB, Lou XW, Wang X (2016) A metal–organic framework-derived bifunctional oxygen electrocatalyst. Nat Energy 1:15006

[30] Huang Y, Liang J, Wang X, Cao R (2017) Multifunctional metal–organic framework catalysts: synergistic catalysis and tandem reactions. Chem Soc Rev 46:126–157

[31] Kaneti Y, Tang J, Salunkhe R, Jiang X, Yu A, Wu K, Yamauchi Y (2017) Nanoarchitectured design of porous materials and nanocomposites from metal–organic frameworks. Adv Mater 29:1604898

[32] Zhu L, Liu XQ, Jiang HL, Sun LB (2017) Metal–organic frameworks for heterogeneous basic catalysis. Chem Rev 117:8129–8176

[33] Xu J, Lawson T, Fan H, Su D, Wang G (2018) Updated metal compounds (MOFs, S, OH, N, C) used as cathode materials for lithium–sulfur batteries. Adv Energy Mater 8:1702607

[34] Kitao T, Zhang Y, Kitagawa S, Wang B, Uemura T (2017) Hybridization of MOFs and polymers. Chem Soc Rev 46:3108–3133

[35] Furukawa H, Cordova KE, O'Keeffe M, Yaghi OM (2013) The chemistry and applications of metal–organic frameworks. Science 341:1230444

[36] Fang X, Jiao L, Yu SH, Jiang HL (2017) Metal–organic framework-derived FeCo–N-doped hollow porous carbon nanocubes for electrocatalysis in acidic and alkaline media. Chem Sus Chem 10:3019–3024

[37] Li X, Jiang Q, Dou S, Deng L, Huo J, Wang S (2016) ZIF-67-derived Co–NC@CoP–NC nanopolyhedra as an efficient bifunctional oxygen electrocatalyst. J Mater Chem A 4:15836–15840

[38] Hu H, Han L, Yu M, Wang Z, Lou XW (2016) Metal–organic-framework-engaged formation of Co nanoparticle-embedded carbon@Co9S8 double-shelled nanocages for efficient oxygen reduction. Energy Environ Sci 9:107–111

[39] Wang J, Jing X, Cao Y, Li G, Huo Q, Liu Y (2015) Structural diversity and magnetic properties of three metal–organic frameworks assembled from a T-shaped linker. Cryst Eng Commun 17:604–611

[40] Liu Y, Hu Y, Zhou M, Qian H, Hu X (2012) Microwave-assisted non-aqueous route to deposit well-dispersed ZnO nanocrystals on reduced graphene oxide sheets with improved photoactivity for the decolorization of dyes under visible light. Appl Catal B Environ 125:425–431

[41] Hu W, Wang Q, Wu S, Huang Y (2016) Facile one-pot synthesis of a nitrogen-doped mesoporous carbon architecture with cobalt oxides encapsulated in graphitic layers as a robust bicatalyst for oxygen reduction and evolution reactions. J Mater Chem A 4:16920–16927

[42] Jiang H, Liu Y, Li W, Li J (2018) Co nanoparticles confined in 3D nitrogen-doped porous carbon foams as bifunctional electrocatalysts for long-life rechargeable Zn–air batteries. Small 14:1703739

[43] Guo C, Liao W, Li Z, Chen C (2015) Exploration of the catalytically active site structures of animal biomass-modified on cheap carbon nanospheres for oxygen reduction reaction with high activity, stability and methanol-tolerant performance in alkaline medium. Carbon 85:279–288

[44] Wu Z, Xu X, Hu B, Liang H, Lin Y, Chen L, Yu SH (2015) Iron carbide nanoparticles encapsulated in mesoporous Fe–N-doped carbon nanofibers for efficient electrocatalysis. Angew Chem Int Ed 127:8297–8301

[45] Guo C, Hu R, Liao W, Li Z, Sun L, Shi D, Li Y, Chen C (2017) Protein-enriched fish "biowaste" converted to three-dimensional porous carbon nano-network for advanced

oxygen reduction electrocatalysis. Electrochim Acta 236:228–238

[46] Yoon KR, Choi J, Cho SH, Jung JW, Kim C, Cheong JY, Kim ID (2018) Facile preparation of efficient electrocatalysts for oxygen reduction reaction: one-dimensional meso/macroporous cobalt and nitrogen Co-doped carbon nanofibers. J Power Sources 380:174–184

[47] Tan AD, Wan K, Wang YF, Fu ZY, Liang ZX (2018) N, S-containing MOF-derived dual-doped mesoporous carbon as a highly effective oxygen reduction reaction electrocatalyst. Catal Sci Technol 8:335–343

[48] Liu Y, Jiang H, Zhu Y, Yang X, Li C (2016) Transition metals (Fe Co, and Ni) encapsulated in nitrogen-doped carbon nanotubes as bi-functional catalysts for oxygen electrode reactions. J Mater Chem A 4:1694–1701

[49] Zhang E, Xie Y, Ci S, Jia J, Cai P, Yi L, Wen Z (2016) Multifunctional high-activity and robust electrocatalyst derived from metal–organic frameworks. J Mater Chem A 4:17288–17298

[50] Yang W, Liu X, Chen L, Liang L, Jia J (2017) A metal–organic framework devised Co–N doped carbon microsphere/nanofiber hybrid as a free-standing 3D oxygen catalyst. Chem Commun 53:4034–4037

[51] Chen Y, Guo Y, Cui H, Xie Z, Zhang X, Wei J, Zhou Z (2018) Bifunctional electrocatalysts of MOF-derived Co–N/C on bamboo-like MnO nanowires for high-performance liquid- and solid-state Zn–air batteries. J Mater Chem A 6:9716–9722

[52] Guan B, Yu L, Lou XW (2017) Formation of single-holed cobalt/N-doped carbon hollow particles with enhanced electrocatalytic activity toward oxygen reduction reaction in alkaline media. Adv Sci 4:1700247

[53] You B, Jiang N, Sheng M, Drisdell WS, Yano J, Sun Y (2015) Bimetal–organic framework self-adjusted synthesis of support-free nonprecious electrocatalysts for efficient oxygen reduction. ACS Catal 5:7068–7076

[54] Li Z, Zhao D, Xu C, Ning J, Zhong Y, Zhang Z, Wang Y, Hu Y (2018) Reduced $CoNi_2S_4$ nanosheets with enhanced conductivity for high-performance supercapacitors. Electrochim Acta 278:33–41

[55] Hu E, Ning J, He B, Li Z, Zheng C, Zhong Y, Zhang Z, Hu Y (2017) Unusual formation of tetragonal microstructures from nitrogen-doped carbon nanocapsules with cobalt nanocores as a bi-functional oxygen electrocatalyst. J Mater Chem A 5:2271–2279

[56] Huang L, Zhang X, Han Y, Wang Q, Fang Y, Dong S (2017) In situ synthesis of ultrathin metal–organic framework nanosheets: a new method for 2D metal-based nanoporous carbon electrocatalysts. J Mater Chem A 5:18610–18617

[57] Liang HW, Zhuang X, Brüller S, Feng X, Müllen K (2014) Hierarchically porous carbons with optimized nitrogen doping as highly active electrocatalysts for oxygen reduction. Nat Commun 5:4973

[58] Deng D, Pan X, Yu L, Cui Y, Jiang Y, Qi J, Li WX, Fu Q, Ma X, Xue Q, Sun G, Bao X (2011) Toward N-doped graphene via solvothermal synthesis. Chem Mater 23:1188–1193

[59] Guo C, Li Y, Liao W, Liu Y, Li Z, Sun L, Chen C, Zhang J, Si Y, Li L (2018) Boosting the oxygen reduction activity of a three-dimensional network Co–N–C electrocatalyst via space-confined control of nitrogen-doping efficiency and the molecular-level coordination effect. J Mater Chem A 6:13050–13061

[60] Nandan R, Nanda KK (2017) Designing N-doped carbon nanotubes and Fe–Fe_3C nanostructures Co-embedded in B-doped mesoporous carbon as an enduring cathode electrocatalyst for metal–air batteries. J Mater Chem A 5:16843–16853

[61] Lai L, Potts JR, Zhan D, Wang L, Poh C, Tang C, Gong H, Shen Z, Lin J, Ruoff R (2012) Exploration of the active center structure of nitrogen-doped graphene-based catalysts for oxygen reduction reaction. Energy Environ Sci 5:7936–7942

[62] Hu F, Yang H, Wang C, Zhang Y, Lu H, Wang Q (2017) Co–N-doped mesoporous carbon hollow spheres as highly efficient electrocatalysts for oxygen reduction reaction. Small 13:1602507